



Expected magnitude of the aerosol shortwave indirect effect in springtime Arctic liquid water clouds

Dan Lubin¹ and Andrew M. Vogelmann²

Received 10 November 2006; revised 16 January 2007; accepted 23 April 2007; published 2 June 2007.

[1] Radiative transfer simulations are used to assess the expected magnitude of the diurnally-averaged shortwave aerosol first indirect effect in Arctic liquid water clouds, in the context of recently discovered longwave surface heating of order 3 to 8 W m⁻² by this same aerosol effect detected at the Barrow, Alaska, ARM Site. We find that during March and April, shortwave surface cooling by the first indirect effect is comparable in magnitude to the longwave surface heating. During May and June, the shortwave surface cooling exceeds the longwave heating. Due to multiple reflection of photons between the snow or sea ice surface and cloud base, the shortwave first indirect effect may be easier to detect in surface radiation measurements than from space. **Citation:** Lubin, D., and A. M. Vogelmann (2007), Expected magnitude of the aerosol shortwave indirect effect in springtime Arctic liquid water clouds, *Geophys. Res. Lett.*, 34, L11801, doi:10.1029/2006GL028750.

[2] The search for indirect aerosol effects has taken a unique turn in the Arctic, in emphasizing longwave radiation before shortwave [Garrett *et al.*, 2002]. This is in part due to the greater importance of longwave radiation relative to shortwave at high latitudes [e.g., Intrieri *et al.*, 2002], and also due to the availability of high quality longwave spectral radiation measurements in the Arctic from which the indirect effect can be readily identified [Garrett and Zhao, 2006; Lubin and Vogelmann, 2006]. To date, the deployment in the high Arctic of advanced longwave spectroradiometers [Turner *et al.*, 2003; Knuteson *et al.*, 2004] has not been matched by similar instrumentation that cover the visible through near-IR wavelengths at which clouds both absorb and scatter radiation. We therefore do not yet have a comparable spectral capability in the Arctic to rigorously identify and quantify the shortwave aerosol for all applicable liquid water paths (*LWP*), as has been done recently for the longwave. The purpose of this study is to demonstrate the expected relative importance of the shortwave and longwave manifestations of the aerosol first indirect effect on the springtime Arctic radiative energy balance.

[3] Garrett and Zhao [2006] analyzed Fourier Transform Infrared (FTIR) spectroradiometer data from the U.S. Department of Energy Atmospheric Radiation Measurement (ARM) program North Slope of Alaska (NSA) site at Barrow, Alaska, and found that the presence of Arctic “haze” – an anthropogenic aerosol primarily of Eurasian industrial origin trapped in the Arctic winter and spring

troposphere [Barrie, 1986] – reduces the mean effective droplet radius r_e of Arctic liquid water clouds by 3 μm . This results in an increase in mean cloud emissivity for all $LWP < 80 \text{ g m}^{-2}$ such that downwelling longwave radiation at the Arctic surface increases by 3.3 to 5.5 W m⁻², with all other meteorological variables held constant. Lubin and Vogelmann [2006] performed a similar analysis of NSA FTIR spectroradiometer data, and found a reduction in mean cloud droplet effective radius of 4 μm in Arctic haze relative to background aerosol, and found an increase of 8.2 W m⁻² in the downwelling surface longwave flux under liquid water clouds in the presence of Arctic haze versus background aerosol, of which 3.4 W m⁻² was attributable to the r_e change alone. Since these results indicate that the first indirect effect operates in these clouds, a concomitant cooling effect is expected in the shortwave [e.g., Penner *et al.*, 2004].

[4] Based on the above-mentioned analyses of ARM FTIR data, we consider how a change in effective droplet radius in Arctic liquid water clouds from a “clean air” value of 11 μm [Tsay *et al.*, 1989] to an observed Arctic Haze value of 8 μm is expected to impact the diurnally averaged shortwave radiation budget. Our results are dependent on this assumed climatological r_e difference, which may be subject to revision from ongoing work in this area. We note that r_e differences ranging from 1–7 μm appear in the literature in studies that compare spring versus summer states [Dong and Mace, 2003; Shupe *et al.*, 2005] or that report case studies [Hobbs and Rangno, 1998; Zuidema *et al.*, 2005]. However, the above-mentioned ARM FTIR studies are to date the only ones giving climatological (multiyear) r_e differences specifically for clouds in clean air versus Arctic haze (determined explicitly from aerosol loading observations); thus, a 3 μm r_e difference is presently the most defensible choice for this study. We consider here only the first indirect effect, or “Twomey effect” [e.g., Garrett *et al.*, 2002], which involves changes in cloud reflectance and absorption due to changes in r_e . The second indirect effect, related to increasing cloud lifetime with decreasing r_e [Albrecht, 1989], is beyond the scope of this paper and has not yet been detected in the Arctic.

[5] We use a 179-band shortwave discrete-ordinates radiative transfer model [Stamnes *et al.*, 1988] that has been used for a variety of high latitude and tropical simulations and data analyses [Lubin *et al.*, 1996; Lubin and Simpson, 1997; Pope and Valero, 2000]. We use a liquid water cloud with lognormal droplet size distribution, with base height and geometrical thickness both 500 m. Commensurate with the changes in r_e , changes in droplet concentration were accounted for when computing the cloud single scattering albedo, asymmetry factor, and volume extinction coefficients. Consistent with observations of

¹Scripps Institution of Oceanography, University of California, San Diego, La Jolla, California, USA.

²Brookhaven National Laboratory, Upton, New York, USA.

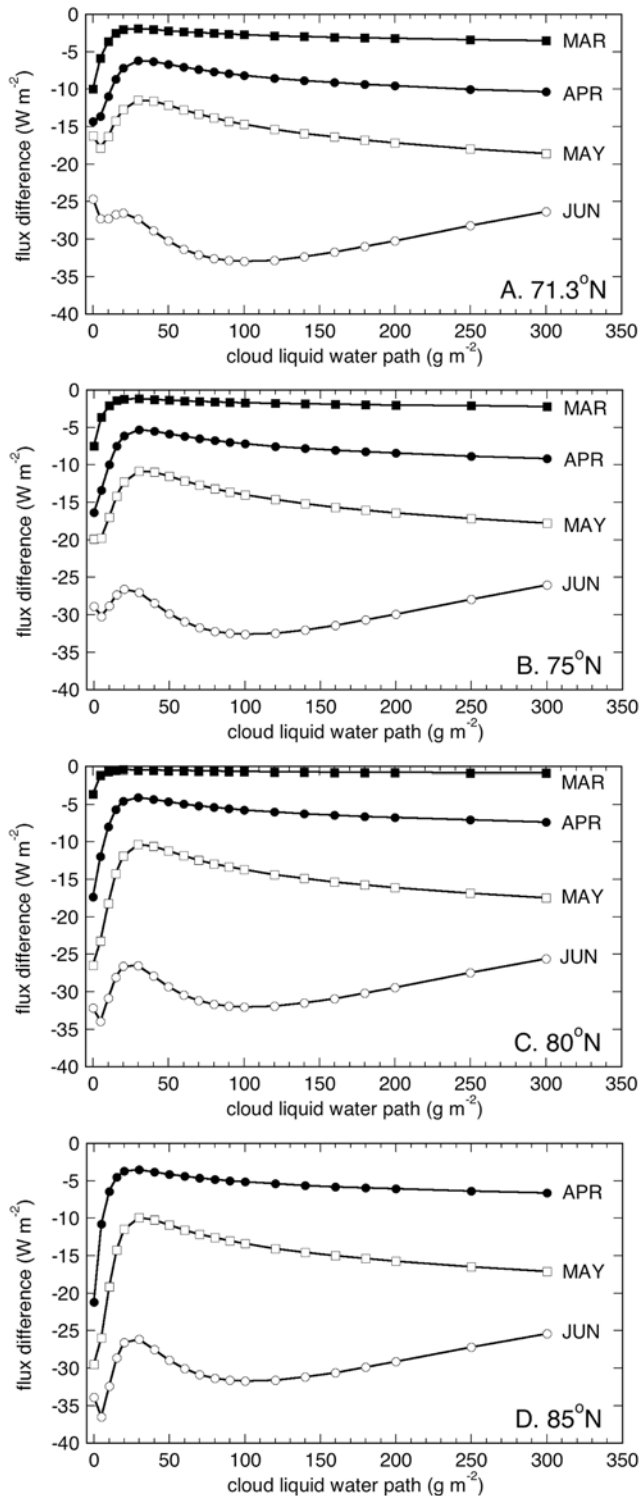


Figure 1. The difference in broadband diurnally averaged downwelling surface shortwave flux due to a change in cloud effective droplet radius r_e from $11 \mu\text{m}$ to $8 \mu\text{m}$, combined with a change in aerosol burden from 500 nm optical depth $\tau_a = 0.1$ to $\tau_a = 0.5$, as a function of cloud liquid water path, for the middle of each month during spring (March to June). Shown for (a) the latitude of Barrow, Alaska, and (b, c, d) latitudes farther north.

significant Arctic haze opacity at aircraft altitudes [e.g., Dutton *et al.*, 1989], which indicate that Arctic haze is not confined to the boundary layer, we specify the aerosol burden as well mixed in the lower 3 km. These same aircraft studies also indicate a wide variety of aerosol layering, both above and below cloud, as opposed to a simple well-mixed scenario. However, this variability in layering is not yet fully understood, and our choice of a well mixed lower troposphere is intended to consider the general and common situation of an Arctic haze concentration that is both within and bracketing a cloud deck. The background aerosol loading is set at 500 nm aerosol optical depth $\tau_a = 0.1$, and polluted aerosol loading is set at $\tau_a = 0.5$, consistent with numerous Arctic field studies (e.g., A. M. Vogelmann *et al.*, manuscript in preparation, 2007). Spectral aerosol optical properties, as a function of relative humidity, are taken from the Arctic haze model of *d'Almeida et al.* [1991]. Surface albedo is specified using measurements from the Surface Heat Budget of the Arctic (SHEBA) experiment [Perovich *et al.*, 2002]; a snow surface is used for March through May, while a bare sea ice cover is used for June (when the melt season generally begins). These radiative transfer simulations, although idealized using a plane-parallel model, are adequate [e.g., Leontyeva and Stamnes, 1994] to demonstrate the basic evolution of the diurnally averaged shortwave first indirect effect throughout the spring season, so that its changing magnitude can be compared with the longwave indirect effect recently determined from ARM NSA measurements.

[6] We demonstrate the shortwave surface manifestation of the indirect effect as the difference in broadband, diurnally-averaged downwelling flux at the surface between the case of a cloud with the smaller effective droplet radius ($8 \mu\text{m}$) in an atmosphere with high aerosol burden, and the case of a cloud with larger effective droplet radius ($11 \mu\text{m}$) in an atmosphere with a background aerosol burden. This flux difference does contain a contribution from direct aerosol extinction (discussed further below), but we include it because the combination of the two effects is what one would actually see in nature. This flux difference is shown in Figure 1 for four high latitudes and four days in the middle of the springtime months, as a function of cloud liquid water path. The flux difference is quite small ($< -5 \text{ W m}^{-2}$) during March, and during early spring may not be easily detected using standard broadband measurements. However, later during spring the flux difference generally drops below -10 W m^{-2} , and during June sometimes exceeds -30 W m^{-2} . The increasing flux difference between March through May is due to increasing solar elevation and day length. During June the lower surface albedo further enhances the flux difference, because there are fewer multiple reflections between surface and cloud base that in the earlier months had partly offset the differences in cloud transmissivity due to different r_e . The shortwave manifestation of the first indirect effect is present for all values of LWP .

[7] Figure 2 shows the corresponding flux differences for the top of atmosphere (TOA). This suggests that the first indirect effect is potentially very difficult to detect from space during early spring, when the cloud is over a snow surface. The diurnally averaged TOA flux difference is $< 5 \text{ W m}^{-2}$ in all cases except during June, where we have

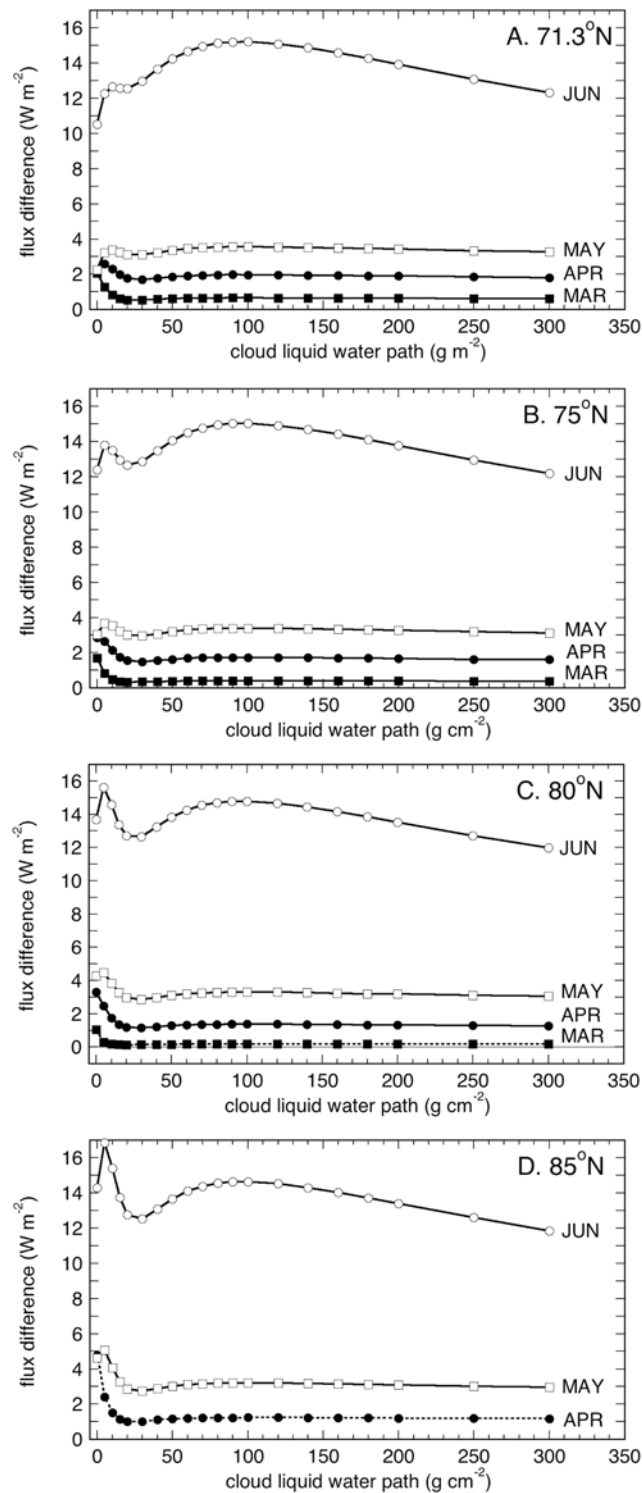


Figure 2. As in Figure 1, but for broadband diurnally averaged upwelling shortwave flux at the top of the atmosphere (TOA).

used a surface albedo representative of bare ice for the melt season. Even here, the TOA flux difference is generally $<15 \text{ W m}^{-2}$. This simulation suggests that verification of the shortwave indirect effect from space over the Arctic might require careful statistical analysis of several years of

satellite Earth radiation budget data, even if concomitant space-based retrievals of thermodynamic phase, r_e , and LWP are available [e.g., Han et al., 1999]. In Figure 1 (and Figure 2), the initial increase then decrease (and vice versa) in the flux differences at low LWP result from the initially greater radiative impact of the aerosol opacity relative to the optically thinnest cloud cover. Also in Figures 1 and 2, we see that the flux difference is not a strong function of cloud opacity at larger LWP ; this is due to the spectrally varying snow/ice albedo [Perovich et al., 2002], which is highest (causing significant multiple reflection) for wavelengths ($<1.0 \mu\text{m}$) at which cloud droplet scattering is conservative, and which decreases significantly at longer wavelengths where cloud droplets absorb and scatter.

[8] A useful way to summarize the climatological significance of Figures 1 and 2 is to consider the LWP distribution observed at NSA for low liquid water clouds. Here we use six years (1998–2003) of NSA microwave radiometer (MWR) data [Liljegren and Lesht, 1996] during March to June, which are screened by the ARM Active Remotely-Sensed Cloud Locations (ARSCL) data set [Clothiaux et al., 2000] for single-layered clouds with both base and geometric thickness $<1000 \text{ m}$. The monthly LWP distributions thus derived are shown in Figure 3, in which we see a gradual shift from smaller to larger LWP from March through June. We also note that the frequency of $LWP > 300 \text{ g m}^{-2}$ is negligible throughout the Arctic spring for these clouds. Although there are 5-years of data used per month, these distributions should be regarded as rough estimates of the month-to-month differences in LWP . This is because recent research has found that MWR uncertainties exist in the LWP retrievals that limit the attainable accuracy to between $20\text{--}30 \text{ g m}^{-2}$ [Liljegren and Lesht, 1996; Westwater et al., 2001; Marchand et al., 2003; Turner et al., 2007], which represents a large uncertainty compared to many of the values shown. Still the shift shown, from smaller to larger LWP from March through June, is consistent with climatological considerations that optically thinner stratiform cloud tend to occur in spring versus summer [e.g., Leontyeva and Stamnes, 1994].

[9] The histograms of Figure 3 were combined with the simulated flux differences as functions of LWP in Figures 1 and 2 to estimate LWP -weighted climatological flux differences for each month and latitude (Table 1). Table 1 also

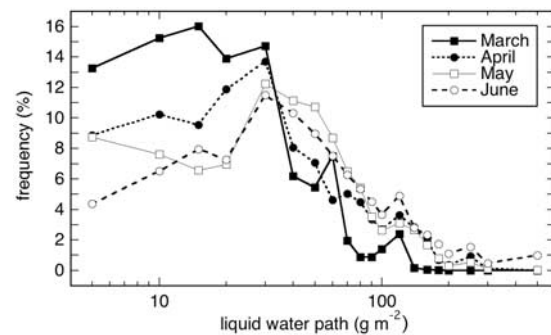


Figure 3. Climatological distribution in liquid water path for single-layer clouds with bases and geometrical thicknesses under 1000 m , estimated from five years of ARM NSA microwave radiometer and ARSCL data.

Table 1. High Versus Low Aerosol Burden Effects on Aerosol Direct and Indirect Effect Fluxes^a

	March		April		May		June	
	clear	cloudy	clear	cloudy	clear	cloudy	clear	cloudy
SFC 85 N			-21.2	-7.2	-29.5	-15.2	-33.9	-29.4
80 N	-3.7	-0.7	-17.4	-7.4	-26.5	-14.9	-32.2	-29.4
75 N	-7.5	-2.0	-16.4	-8.6	-19.9	-14.1	-28.9	-29.3
71.3 N	-10.0	-3.2	-14.3	-9.1	-16.2	-14.0	-24.7	-29.2
TOA 85 N			4.8	1.7	4.6	3.4	14.3	13.8
80 N	1.0	0.2	3.3	1.7	4.3	3.4	13.7	13.7
75 N	1.7	0.5	2.9	1.9	3.0	3.2	12.4	13.7
71.3 N	2.1	0.8	2.2	2.0	2.2	3.2	10.5	13.6

^aSpringtime aerosol direct and indirect shortwave aerosol forcing at mid-month, expressed as the diurnally averaged flux difference between the low aerosol and high aerosol cases, as described in the text. For cloudy skies, the fluxes in both cases are also weighted by the monthly climatological liquid water path in Figure 3. Values given for the downwelling shortwave radiation at the surface (SFC), and at the top of atmosphere (TOA).

lists the clear-sky flux differences, which represent the direct shortwave aerosol effect. These simulated direct aerosol effects are consistent with radiometric measurements from NSA (A. M. Vogelmann et al., manuscript in preparation, 2007).

[10] Our simulation of the diurnally averaged shortwave first indirect effect yields the following conclusions:

[11] (1) A shortwave manifestation of the first indirect effect occurs in liquid water clouds for all LWP observed during the Arctic spring (Figures 1 and 2). This is in contrast to the longwave manifestation, which occurs regardless of solar illumination condition, but only for $\tau_c < \sim 8-10$ and disappears when clouds become optically thick enough to radiate as blackbodies [Lubin and Vogelmann, 2006].

[12] (2) During March and April, the diurnally averaged shortwave cooling caused at the surface by the first indirect effect is comparable in magnitude to the cloud-aerosol associated surface longwave heating of ~ 3 to 8 W m^{-2} determined recently from measurements (Table 1). Hence during early spring, the shortwave and longwave manifestations of the first indirect effect may cancel each other in many instances. If the larger longwave heating (8.2 W m^{-2}) suggested by Lubin and Vogelmann [2006] can eventually be attributed to both r_e and LWP changes from aerosol-cloud nucleation [e.g., Morrison et al., 2005], then during March we could conclude that there is a net surface warming due to aerosol influence on clouds. However, during May and June (with increasing insolation), the surface shortwave cooling becomes progressively larger than the longwave heating, such that the net effect at the surface is a cooling that is partially offset by the increased cloud mid-IR emission.

[13] (3) Because of multiple reflection of photons between the high albedo surface and the cloud base, the first indirect effects' TOA signal is much smaller than its surface downwelling signal. During May and June, the surface effect may be detectable in a suitably large and well-characterized broadband or multispectral shortwave data set. The TOA signal may be difficult to detect in Earth radiation budget data prior to the onset of the melt season,

except over open water or other surfaces with much lower albedo than sea ice.

[14] **Acknowledgments.** This research was supported by the Office of Biological and Environmental Research of the U.S. Department of Energy under grant DOE FG0303-ER63538 and KP1201030 as part of the Atmospheric Radiation Measurement (ARM) Program. Data were used from the North Slope of Alaska (NSA) ARM Climate Research Facility (ACRF).

References

- Albrecht, B. A. (1989), Aerosol, cloud microphysics, and fractional cloudiness, *Science*, *245*, 1227–1230.
- Barrie, L. A. (1986), Arctic air pollution: An overview of current knowledge, *Atmos. Environ.*, *20*, 643–663.
- Clothiaux, E. E., et al. (2000), Objective determination of cloud heights and radar reflectivities using a combination of active remote sensors at the ARM CART sites, *J. Appl. Meteorol.*, *39*, 645–665.
- d'Almeida, G., P. Koepke, and E. P. Shettle (1991), *Atmospheric Aerosols: Global Climatology and Radiative Characteristics*, 561 pp., A. Deepak, Hampton, Va.
- Dong, X., and G. G. Mace (2003), Arctic stratus cloud properties and radiative forcing derived from ground-based data collected at Barrow, Alaska, *J. Clim.*, *16*, 445–461.
- Dutton, E. G., J. J. DeLuisi, and G. Herbert (1989), Shortwave aerosol optical depth of Arctic haze measured on board the NOAA WP-3D during AGASP-II, April 1986, *J. Atmos. Chem.*, *9*, 71–79.
- Garrett, T. J., and C. Zhao (2006), Increased Arctic cloud longwave emissivity associated with pollution from mid-latitudes, *Nature*, *440*, 787–789.
- Garrett, T., L. F. Radke, and P. V. Hobbs (2002), Aerosol effects on cloud emissivity and surface longwave heating in the Arctic, *J. Atmos. Sci.*, *59*, 769–778.
- Han, W., K. Stamnes, and D. Lubin (1999), Remote sensing of cloud properties in the Arctic from AVHRR measurements, *J. Appl. Meteorol.*, *38*, 989–1012.
- Hobbs, P. V., and A. L. Rangno (1998), Microstructure of low and middle-level clouds over the Beaufort Sea, *Q. J. R. Meteorol. Soc.*, *124*, 2035–2071.
- Intrieri, J. M., C. W. Fairall, M. D. Shupe, P. O. G. Persson, E. L. Andreas, P. S. Guest, and R. E. Moritz (2002), An annual cycle of Arctic surface cloud forcing at SHEBA, *J. Geophys. Res.*, *107*(C10), 8039, doi:10.1029/2000JC000439.
- Knuteson, R. O., et al. (2004), Atmospheric emitted radiance interferometer. part II: Instrument performance, *J. Atmos. Oceanic Technol.*, *21*, 1777–1789.
- Leontyeva, E., and K. Stamnes (1994), Estimations of cloud optical thickness from ground-based measurements of incoming solar radiation in the Arctic, *J. Clim.*, *7*, 566–578.
- Liljegren, J. C., and B. M. Lesht (1996), Measurements of integrated water vapor and cloud liquid water from microwave radiometers at the DOE ARM cloud and radiation testbed in the southern Great Plains, paper presented at International Geoscience Remote Sensing Symposium, IEEE, Lincoln, Nebr., 21–26 May.
- Lubin, D., and A. S. Simpson (1997), Measurement of surface radiation fluxes and cloud optical properties during the 1994 Arctic Ocean Section, *J. Geophys. Res.*, *102*, 4275–4286.
- Lubin, D., and A. M. Vogelmann (2006), A climatologically significant aerosol longwave indirect effect in the Arctic, *Nature*, *439*, 453–456.
- Lubin, D., J.-P. Chen, P. Pilewskie, V. Ramanathan, and F. P. J. Valero (1996), Microphysical examination of excess cloud absorption in the tropical atmosphere, *J. Geophys. Res.*, *101*, 16,961–16,972.
- Marchand, R., T. Ackerman, E. R. Westwater, S. A. Clough, K. Cady-Pereira, and J. C. Liljegren (2003), An assessment of microwave absorption models and retrievals of cloud liquid water using clear-sky data, *J. Geophys. Res.*, *108*(D24), 4773, doi:10.1029/2003JD003843.
- Morrison, H., J. A. Curry, M. D. Shupe, and P. Zuidema (2005), A new double-moment microphysics parameterization for application in cloud and climate models. part II: Single-column modeling of Arctic clouds, *J. Atmos. Sci.*, *62*, 1678–1693.
- Penner, J. E., X. Dong, and Y. Chen (2004), Observational evidence of a change in radiative forcing due to the aerosol indirect effect, *Nature*, *427*, 231–234.
- Perovich, D. K., T. C. Grenfell, B. Light, and P. V. Hobbs (2002), Seasonal evolution of the albedo of multiyear Arctic sea ice, *J. Geophys. Res.*, *107*(C10), 8044, doi:10.1029/2000JC000438.
- Pope, S. K., and F. P. J. Valero (2000), Observations and models of irradiance profiles, column transmittance, and column reflectance during the

- Atmospheric Radiation Measurements Enhanced Shortwave Experiment, *J. Geophys. Res.*, *105*, 12,521–12,528.
- Shupe, M. D., T. Uttal, and S. Y. Matrosov (2005), Arctic cloud microphysics retrievals from surface-based remote sensors at SHEBA, *J. Appl. Meteorol.*, *44*, 1544–1562.
- Stamnes, K., S.-C. Tsay, W. J. Wiscombe, and K. Jayaweera (1988), Numerically stable algorithm for discrete-ordinate-method radiative transfer in multiple scattering and emitting layered media, *Appl. Opt.*, *27*, 2502–2509.
- Tsay, S.-C., K. Stamnes, and K. Jayaweera (1989), Radiative energy budget in the cloudy and hazy Arctic, *J. Atmos. Sci.*, *46*, 1002–1018.
- Turner, D. D., S. A. Ackerman, B. A. Baum, H. E. Revercomb, and P. Yang (2003), Cloud phase determination using ground-based AERI observations at SHEBA, *J. Appl. Meteorol.*, *42*, 701–715.
- Turner, D. D., et al. (2007), Thin liquid water clouds: Their importance and our challenge, *Bull. Am. Meteorol. Soc.*, *88*, 177–190.
- Westwater, E. R., Y. Han, M. D. Shupe, and S. Matrosov (2001), Analysis of integrated cloud liquid water and precipitable water vapor retrievals from microwaver radiometers during the Surface Heat Budget of the Arctic Ocean project, *J. Geophys. Res.*, *106*, 32,019–32,030.
- Zuidema, P., B. Baker, Y. Han, J. Intrieri, J. Key, P. Lawson, S. Matrosov, M. Shupe, R. Stone, and T. Uttal (2005), An Arctic springtime mixed-phase cloudy boundary layer observed during SHEBA, *J. Atmos. Sci.*, *62*, 170–176.
-
- D. Lubin, Scripps Institution of Oceanography, University of California, San Diego, 9500 Gilman Drive, La Jolla, CA 92093, USA. (dlubin@ucsd.edu)
- A. M. Vogelmann, Brookhaven National Laboratory, Upton, NY 11973, USA.